Geochemistry, Geophysics, Geosystems

Supporting Information for

Volcano Deformation Survey over the Northern and Central Andes with ALOS InSAR Time Series

Anieri M. Morales Rivera[1], Falk Amelung[1], and Patricia Mothes[2]

[1]Rosenstiel School of Marine and Atmospheric Science, University of Miami, Miami, FL, USA.

[2]Instituto Geofisico, Escuela Politecnica Nacional, Casilla 1701-2759, Quito, Ecuador.

Contents of this file

Additional Supporting Information (Files uploaded separately)

Captions for Data Set S1

Introduction

Volcanoes over the study area with confirmed magmatic eruptions from 2006-2011 are presented in Table S1. The best fitting source parameters and 95% confidence intervals for deformation at the volcanoes of interest are presented in Tables S2-S5. Examples of eliminated ALOS interferograms due to ionospheric disturbances are included in Text S1 and Figure S1. Explanations and illustrations that demonstrate the applicability of the DEM error correction over our deforming volcanoes, and an illustrated example of the DEM error due to the perpendicular baseline are found in Text S2 and Figures S2-S3. The reference pixel comparison approach is explained in Text S3, with an illustrated example over Guagua Pichincha and Atacazo volcanoes in Figure S4. The time series results over the deforming volcanoes are included in Text S4 and Figures S5-S10. The mean 2007-2011 LOS velocity maps over selected deforming volcanoes, with profiles through the deforming region and surroundings superimposed on the topography, are included in Text S5 and Figures S11-S13.

Volcano	Country	Eruption Start Date	Eruption End Date
Galeras	Colombia	11/24/2005 10/04/2007 10/21/2008? 08/25/2010	07/12/2006 01/17/2008 01/02/2010? 08/25/2010
Nevado del Huila	Colombia	02/19/2007 01/02/2008 10/26/2008?	05/28/2007? 04/??/2008? 01/14/2012?
Reventador	Ecuador	03/15/2007? 07/27/2008	10/11/2007? 06/30/2015-(Continuing)
Sangay	Ecuador	08/08/1934	03/03/2015-(Continuing)
Tungurahua	Ecuador	10/05/1999 01/01/2010 11/22/2010	07/08/2009? 07/29/2010 10/06/2014
Ubinas	Peru	03/25/2006?	07/04/2009?

Table S1. Volcanoes over the study area with confirmed magmatic eruptions from 2006-2011 according to [*Siebert and Simkin*, 2002-2015].

Galeras - Okada Sill

Depth[a] (km): -3.63 ± 0.03 [1.00 to 4.50]
Length (km): 1.76 ± 0.03 [1.50 to 5.00]
Width (km): 3.78 ± 0.08 [2.50 to 5.00]
X_East (km): 7.40 ± 0.04 [4.00 to 7.40]
Y_North (km): 6.77 ± 0.02 [3.50 to 7.40]
Strike (°): 0.01 ± 0.22 [0.01 to 60.00]
Dip (°): 37.0 ± 0.19 [-20.00 to 37.00]
Opening (m): -0.17 ± $5.80*10^{-3}$ [-2.00 to -0.01]
Volume Change (m^3): $-1.2*10^6$

InSAR data: 08/05/2007-09/28/2010 LOS displacement; ALOS T 153, F 0010
Subset (N, W; S, E): 1.28°, -77.39°; 1.18°, -77.29°
RMS (mm): 18.27

[a]Depth is expressed with respect to the lowest elevation of the subset (2028 m). Positive and Negative values are above and below reference elevation respectively.

Table S2. Best fitting source parameters and 95% confidence intervals for deformation at Galeras volcano. The range of modeled source parameters are shown in the brackets.

Guagua Pichincha - Mogi	
Depth[a] (km): -0.52 ± 0.60 [0.30 to -3.00]	**X_East (km)**: 4.88 ± 0.24 [4.00 to 5.20]
Volume Change (10^6 m^3): 0.12 ± 2.00 [0.00 to 999.00]	**Y_North (km)**: 3.95 ± 0.20 [3.50 to 4.80]

InSAR data: 12/23/2006-08/15/2009 LOS displacement; ALOS T 110, F 7170
Subset (N, W; S, E): -0.14°, -78.66°; -0.21°, -78.58°
RMS (mm): 9.72

[a]Depth is expressed with respect to the lowest elevation of the subset (2346 m). Positive and Negative values are above and below reference elevation respectively.

Table S3. Best fitting source parameters and 95% confidence intervals for deformation at Guagua Pichincha volcano. The range of modeled source parameters are shown in the brackets.

Tungurahua – Yang (Shallow Soure)	
Depth (km): 0.72 ± 0.04 [0.80 to -0.50]	**X_East (km)**: 10.17 ± 0.02 [8.60 to 10.30]
Major Axis (km): 2.78 ± 0.03 [2.00 to 35.00]	**Y_North (km)**: 9.05 ± 0.00 [8.90 to 9.15]
Minor Axis (km): 1.08 ± 5.64 x 10^{-4} [0.00 to 5.56]	**Strike (°)**: 87.0 ± 0.22 [87.00 to 95.00]
Pressure Change (μ*Pa): $0.08*10^{-5}$ ± $0.78*10^{-5}$ [0.00 to 999.00]	**Plunge (°)**: 35.70 ± 0.62 [15.00 to 45.00]

Tungurahua – Okada (Deeper Source)	
Depth[a] (km): -1.63 ± 0.06 [-0.90 to -4.00]	**Strike (°)**: 307.70 ± 0.76 [298.00 to 312.00]
Length (km): 0.30 ± 0.04 [0.20 to 0.80]	**Dip (°)**: -21.92 ± 0.62 [-30.00 to -1.00]
Width (km): 7.65 ± 0.08 [5.00 to 8.20]	**Opening (m)**: 0.79 ± 0.02 [0.06 to 0.90]
X_East (km): 7.83 ± 0.06 [7.00 to 8.05]	**Volume Change (m^3)**: $1.8*10^6$
Y_North (km): 9.93 ± 0.04 [9.50 to 11.00]	

InSAR data: 12/23/2006-06/30/2009 LOS displacement; ALOS T 110, F 7150
Subset (N, W; S, E): -1.39°, -78.55°; -1.55°, -78.40°
RMS (mm): 16.82

[a]Depth is expressed with respect to the lowest elevation of the subset (1678m). Positive and Negative values are above and below reference elevation respectively.

Table S4. Best fitting source parameters and 95% confidence intervals for deformation at Tungurahua volcano. The range of modeled source parameters are shown in the brackets.

SE of Cerro Auquihuato - Okada Sill

Depth[a] (km): -0.42 ± 0.04 [0.20 to -1.00]	**Strike (°)**: 198.86 ± 7.34 [1.00 to 359.00]
Length (km): 1.28 ± 0.05 [1.00 to 2.50]	**Dip (°)**: -10.22 ± 3.10 [-40.00 to 40.00]
Width (km): 1.39 ± 0.07 [1.00 to 2.50]	**Opening (m)**: 0.10 ± 0.01 [0.01 to 0.20]
X_East (km): 2.50 ± 0.04 [2.00 to 4.00]	**Volume Change (m^3)**: $0.2*10^6$
Y_North (km): 3.06 ± 0.06 [2.00 to 4.00]	

InSAR data: 01/16/2007-01/27/2011 LOS displacement; ALOS T 106, F 6870
Subset (N, W; S, E): -15.1135°, -73.1994°; -15.1661°, -73.1439°
RMS (mm): 6.87

[a]Depth is expressed with respect to the lowest elevation of the subset (3249 m). Positive and Negative values are above and below reference elevation respectively.

Table S5. Best fitting source parameters and 95% confidence intervals for deformation 7 km SE of Cerro Auquihuato volcano. The range of modeled source parameters are shown in the brackets.

Text S1.

We observed phase distortions and streaks of decorrelation mainly on interferograms acquired over Ecuador and Peru that we attribute to ionospheric disturbances. We use pair-wise logic to determine the dates that were affected by ionospheric effects. Figure S1a shows an example of an eliminated interferogram acquired over Ecuador showing phase distortions associated to ionospheric disturbances during February 18, 2011. Figure S1b shows an example of an eliminated interferogram acquired over Peru showing streaks of decorrelation associated to ionospheric disturbances during February 26, 2007.

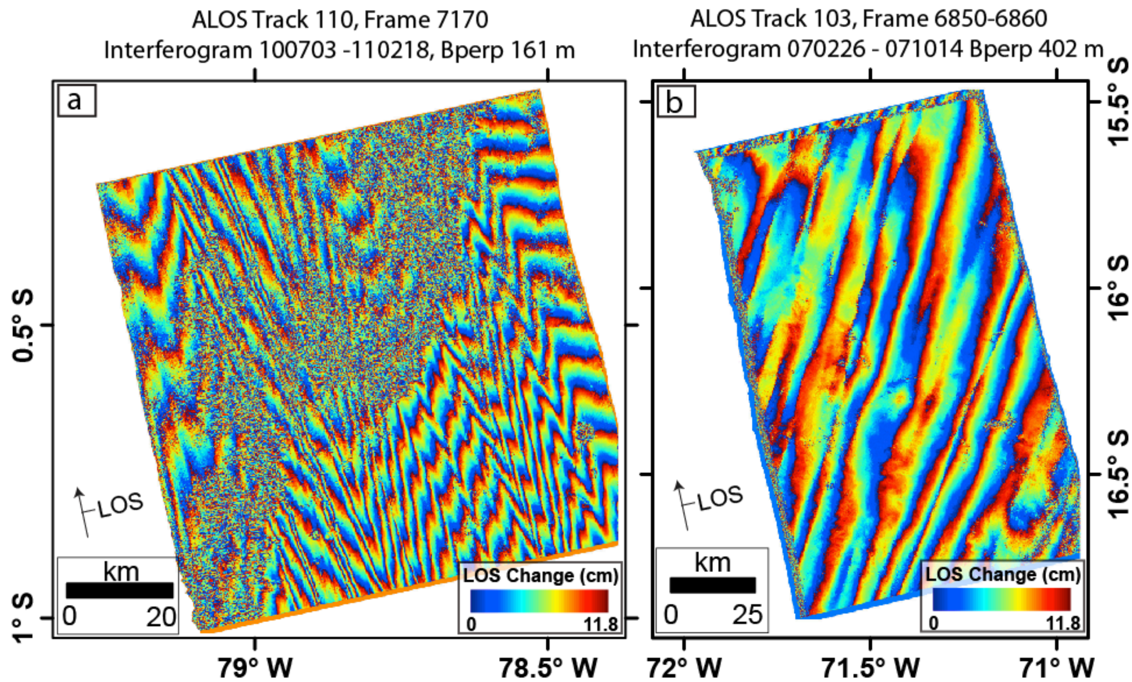

Figure S1. (a) ALOS interferogram from ascending track 110 spanning July 2010 to February 2011 showing phase distortions attributed to ionospheric disturbances, and (b) ALOS interferogram from ascending track 103 spanning February 2007 to October 2007 showing streaks of decorrelation attributed to ionospheric disturbances.

Text S2.

Fattahi and Amelung [2013] demonstrated that the phase due to the DEM error at each epoch is proportional to the perpendicular baseline between the SAR acquisition at that epoch and the reference acquisition.. *Fattahi and Amelung* [2013] presented a model based approach to correct for these DEM errors, with favorable conditions when the uncorrected displacement history is uncorrelated to the perpendicular baseline. Figure S2 illustrates that the DEM error correction can be applied over the 6 deforming volcanoes in our study because the uncorrected displacement history does not correlate with the perpendicular baseline history. Figure S3 illustrates an example of the estimated displacement due to the DEM error from the perpendicular baseline at Reventador volcano. This method does not account for time-dependent topographic changes but it is not a concern because significant changes would result in temporal decorrelation (e.g. observed at Reventador after emplacement of lava flows during the time period of analysis).

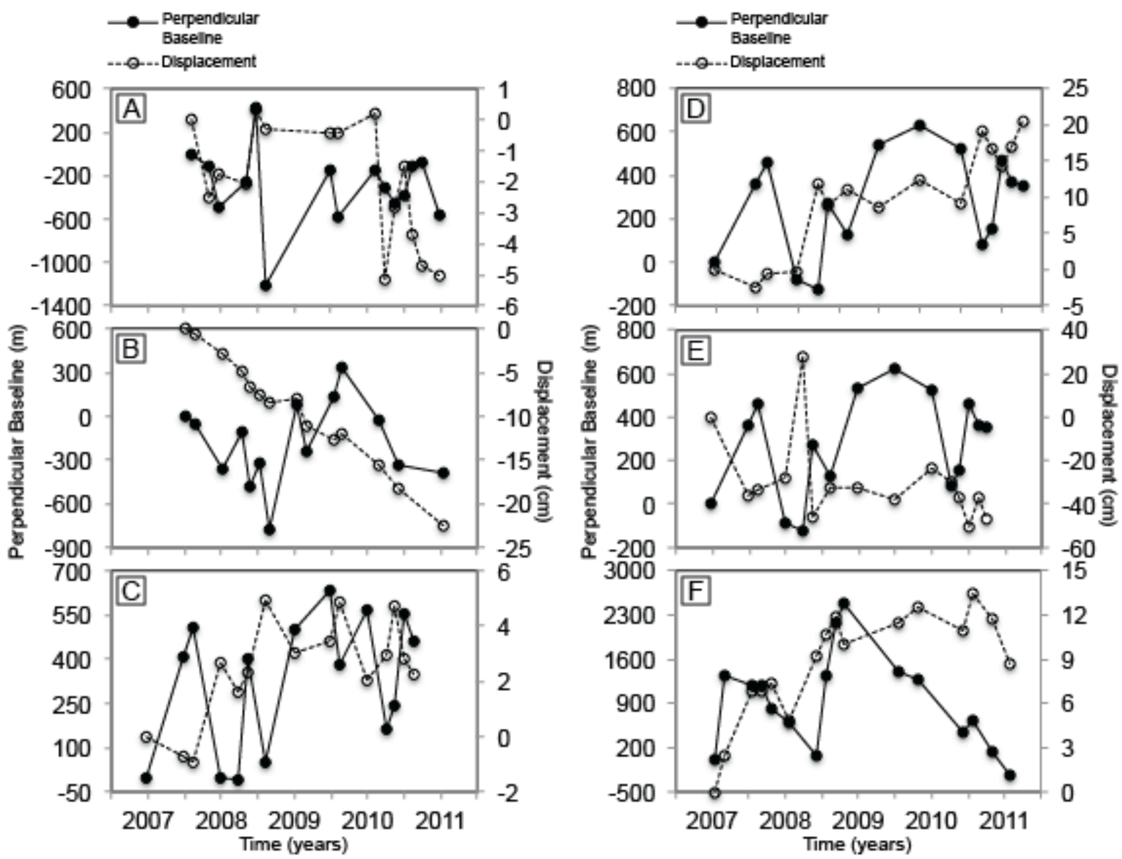

Figure S2. Examples of no correlation between uncorrected displacement time series and perpendicular baselines at (A) Galeras, (B) Reventador, (C) Pichincha, (D) Tungurahua, (E) Sangay, and (F) 7km SE of Cerro Auquihuato.

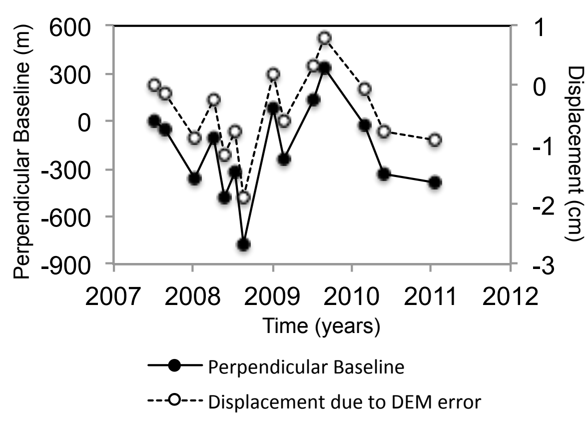

Figure S3. Illustrated example of the estimated displacement history due to the DEM error (difference between the time series with and without DEM error correction) at the same deforming point as in Figure 2 c-d over Reventador volcano, and how it correlates with the perpendicular baseline history.

Text S3.

We investigate the possibility of atmospheric noise reduction of a deforming point by choosing a reference pixel with potentially similar atmospheric conditions. We present an example of this process over Guagua Pichincha (active) and Atacazo (inactive) volcanoes in Figure S4. We first select a random pixel with high temporal coherence in a suspected non-deforming area as the reference pixel. We obtain the LOS displacement time series for three points: (1) in the area of suspected deformation, (2) in a suspected non-deforming area within proximity (≤10 km) to the suspected deformation (to evaluate localized turbulent atmospheric delay), and (3) in a suspected non-deforming area further away (>10 km) from the suspected deformation (to evaluate regional stratified atmospheric delay), with all three points at similar elevations (within ≤ 100 m elevation difference). Temporal correlation of the LOS displacement time series indicate regional stratified atmospheric delays (clearly observed over Guagua Pichincha and Atacazo volcanoes on dates 2-4, 7, 13-15 in Figure S4A). A lack of temporal correlation indicates a real deformation signal and/or the presence of localized atmospheric delay errors (clearly observed in the active dome of Guagua Pichincha, and over Guagua Pichincha and Atacazo on dates 5, 6, 8-12 in Figure S4A). To distinguish between the latter two, we evaluate similarities and differences between the time series. An example is shown in Figure S4A. The time series for Pichincha (black triangle) and Atacazo (black circle) volcanoes are very similar, with slight offsets of ≤2 cm. This suggests that the time series largely represent stratified atmospheric delay while the slight offsets represent the localized turbulent atmospheric delays. The time series on the active dome of Guagua Pichincha (white square) displays some correlation to the other two time series but the difference increases with time, indicating deformation. Assuming that similar localized and regional atmospheric conditions exist within 2 points at proximity, we now use the non-deforming point on the flank of Guagua Pichincha as the reference pixel in order to minimize the atmospheric delays. The trend of the resulting time series represents deformation (white square, Figure S4B).

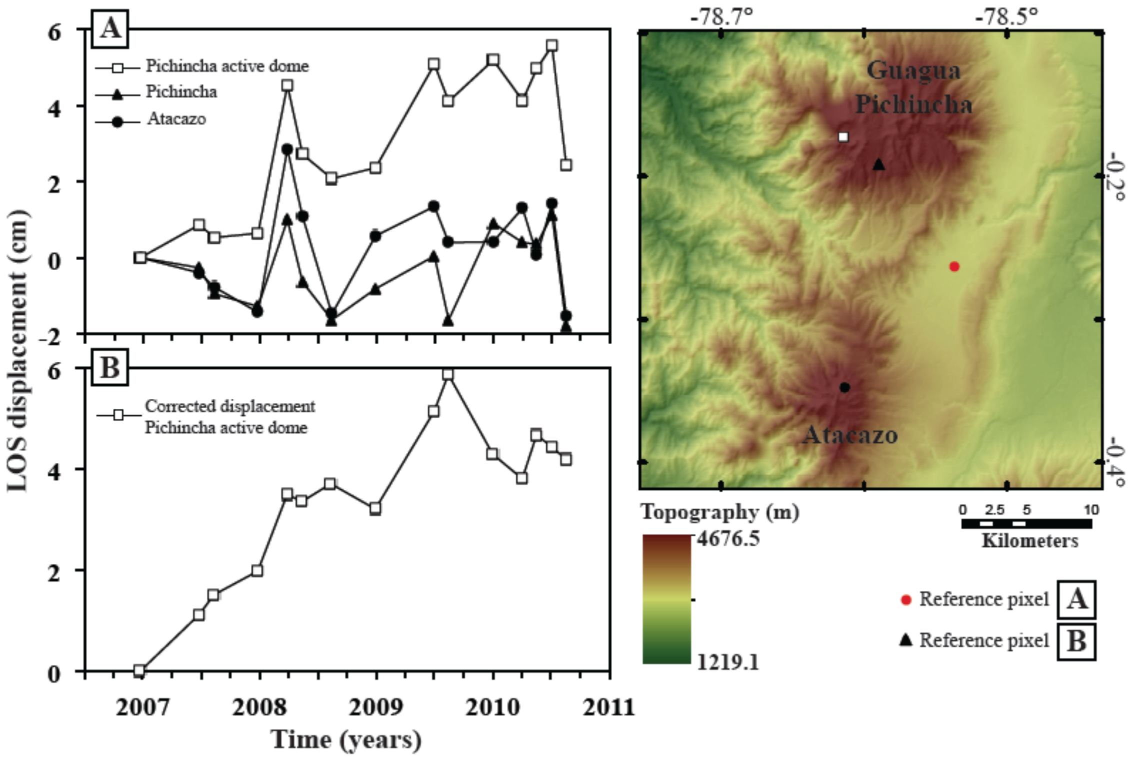

Figure S4. (Left) LOS displacement time series for points on (A) the flanks of Guagua Pichincha (black triangle) and Atacazo (black circle) volcanoes, and the active dome of Guagua Pichincha (white square) with respect to a reference point in Quito (red circle), and (B) the active dome of Guagua Pichincha with respect to a reference point on the flank (black triangle). The DEM (right) shows the location of the points and reference pixels for the time series plots on the left.

Text S4.

We include in Figures S5-S10 the LOS displacement time series over the deforming volcanoes (relative to the first image).

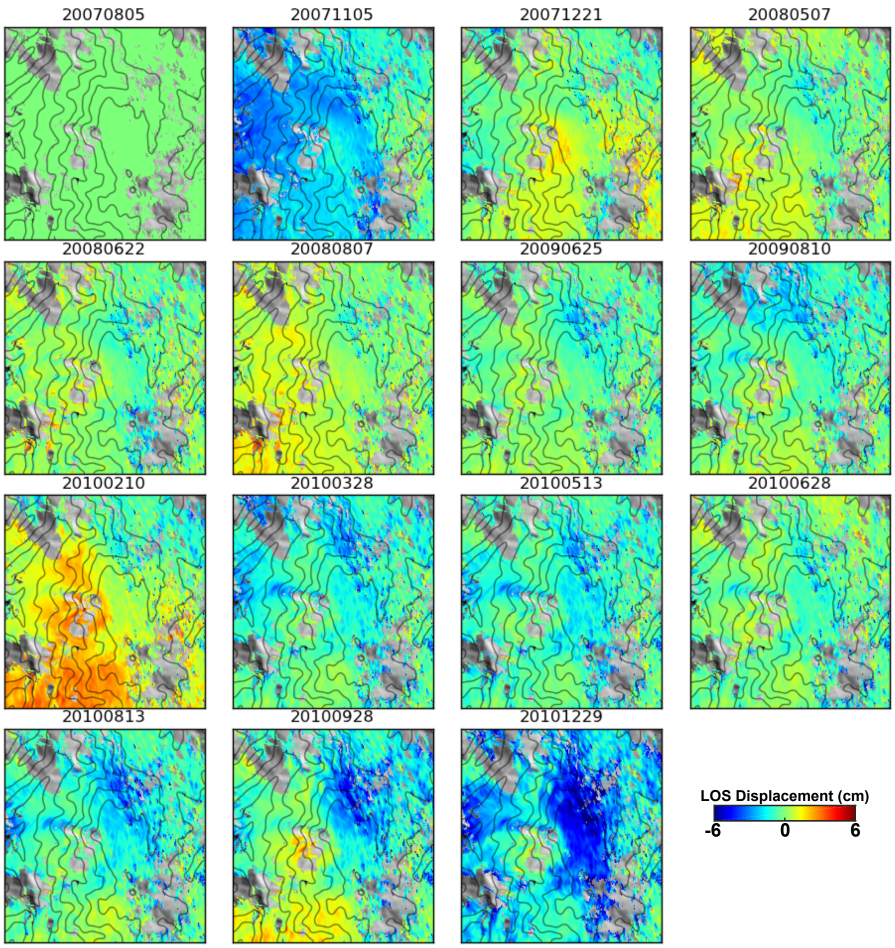

Figure S5. LOS displacement time series over Galeras volcano (Track 153) showing deformation on the NE flank. Area covered over each sub-figure: latitudes 1.265 to 1.18, and longitudes -77.39 to -77.31.

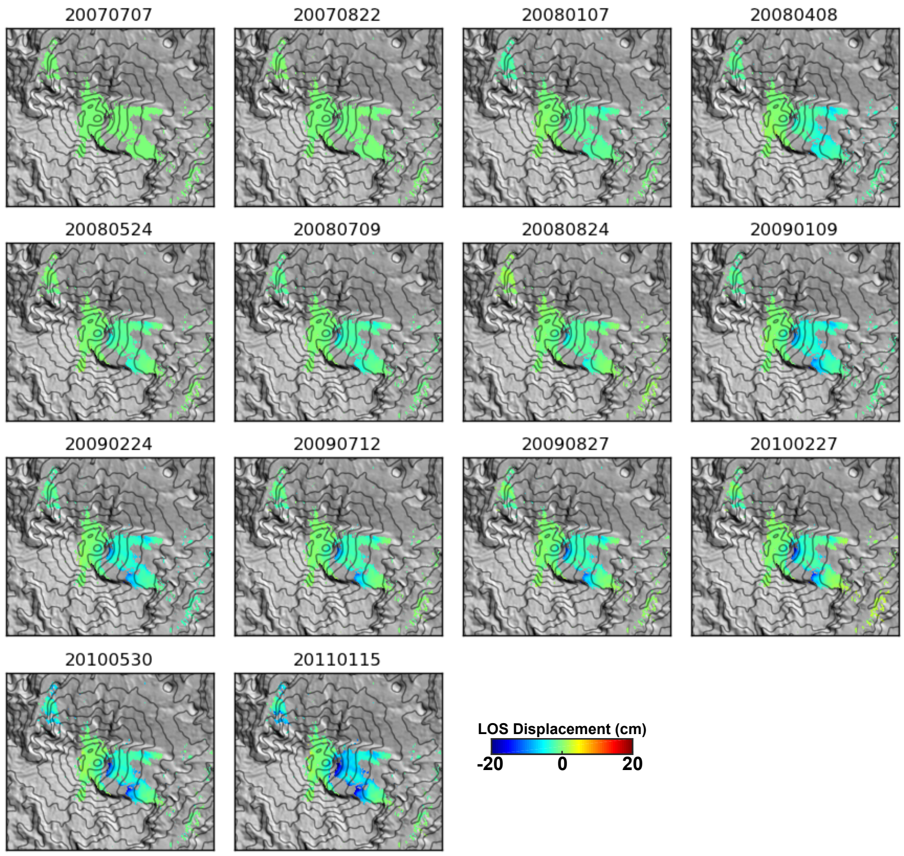

Figure S6. LOS displacement time series over Reventador volcano showing deformation over volcanic deposits emplaced within the sector collapse region (SE flank of the volcano). Area covered over each sub-figure: latitudes -0.02 to -0.14, and longitudes -77.72 to -77.58.

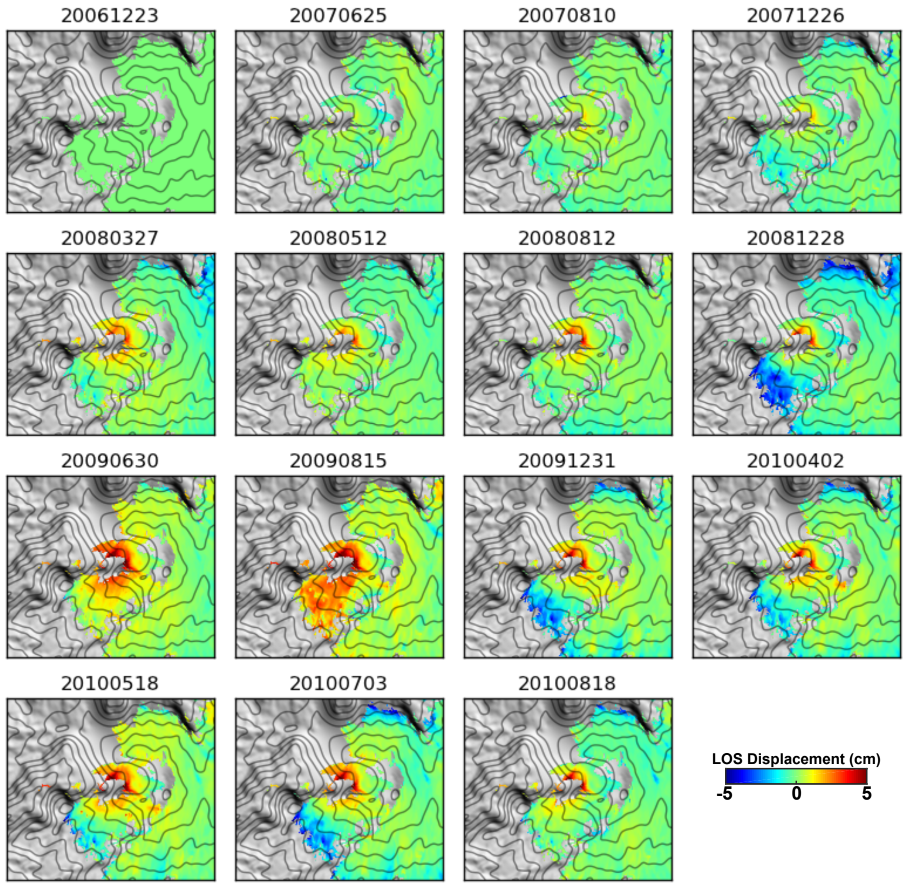

Figure S7. LOS displacement time series over Guagua Pichincha volcano (Track 110) showing deformation on the active dome within the caldera. Area covered over each sub-figure: latitudes -0.14 to -0.21, and longitudes -78.66 to -78.58.

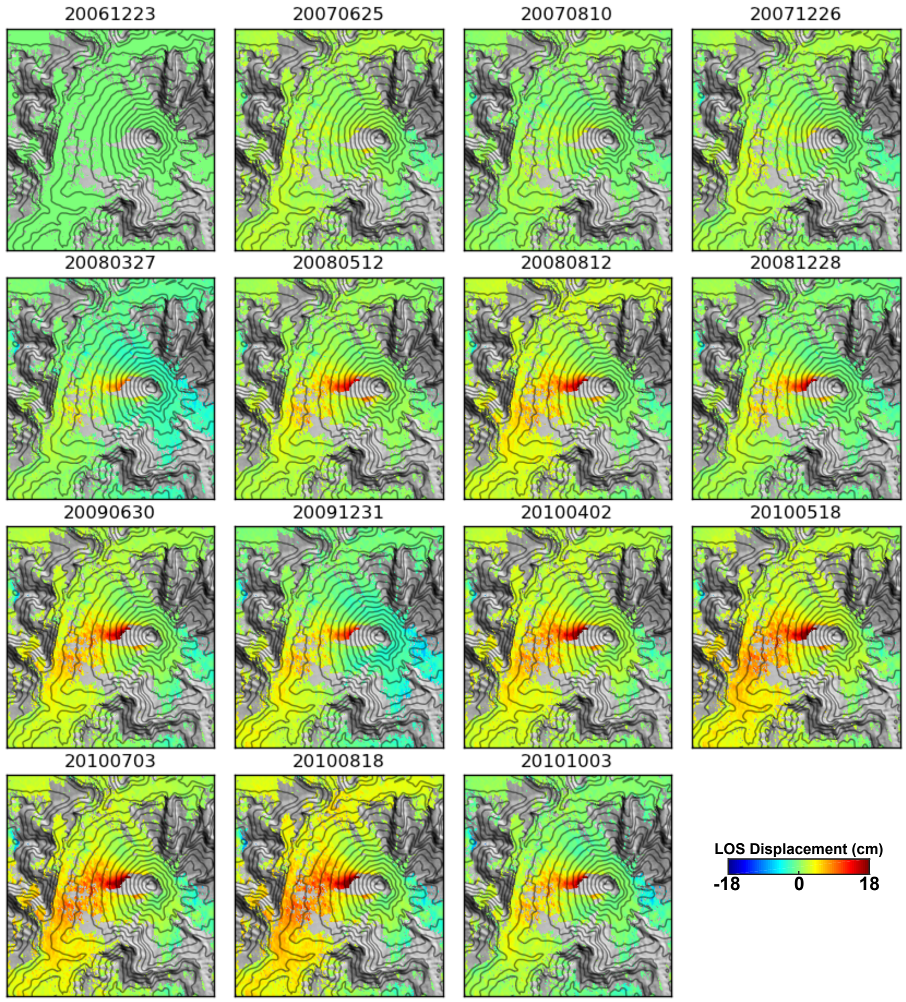

Figure S8. LOS displacement time series over Tungurahua volcano showing deformation on the W flank. Area covered over each sub-figure: latitudes -1.39 to -1.55, and longitudes -78.55 to -78.40.

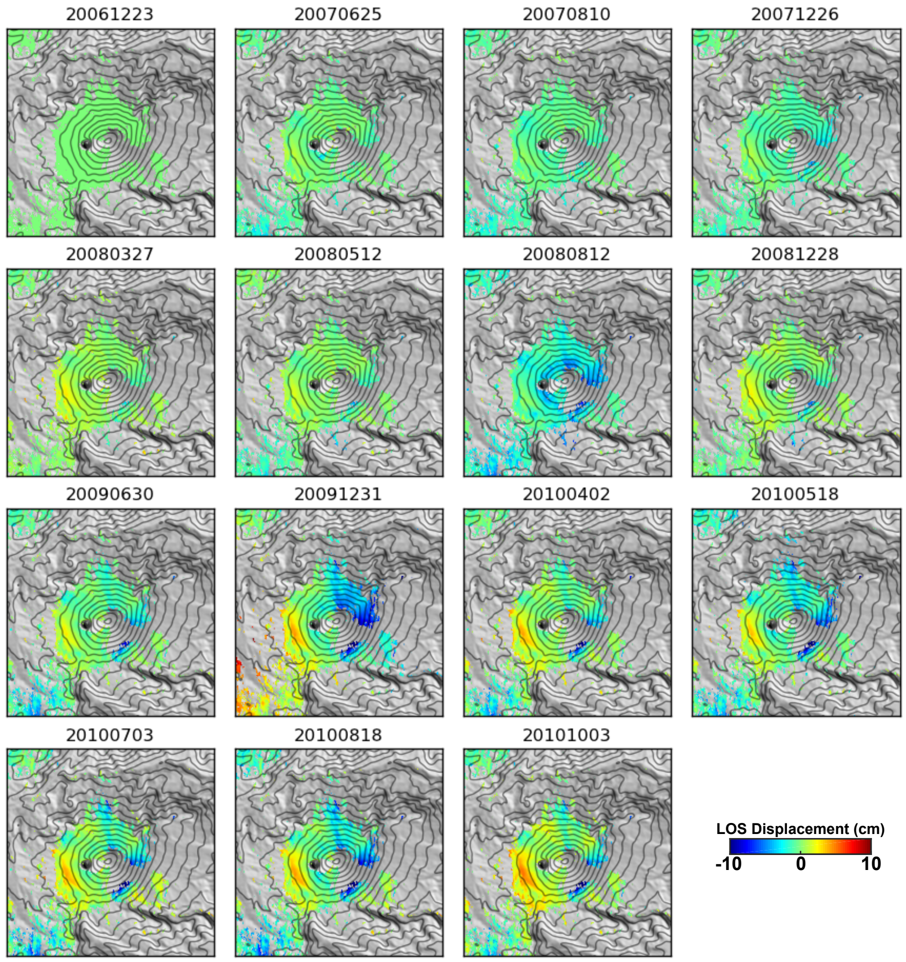

Figure S9. LOS displacement time series over Sangay volcano showing deformation on the SW and SE flanks of the volcano. Area covered over each sub-figure: latitudes -1.94 to -2.06, and longitudes -78.40 to -78.28.

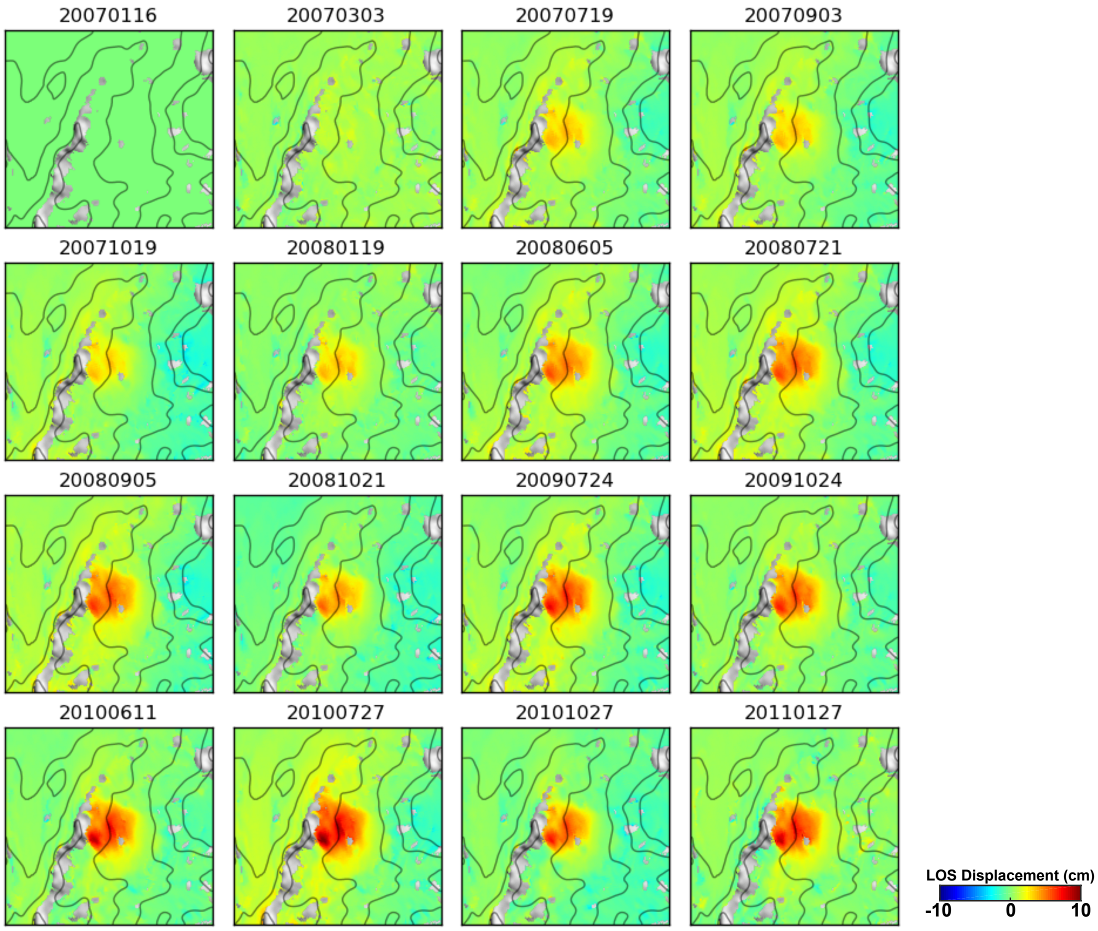

Figure S10. LOS displacement time series 7km SE of Cerro Auquihuato showing deformation. Area covered over each sub-figure: latitudes -15.1135 to -15.1661, and longitudes -73.1994 to -73.1439.

Text S5.

Interpretations based on small regions within the InSAR products need to be evaluated considering that signals of similar magnitude can appear in other regions. We present a larger view of the velocity maps, along with profiles that display the average LOS velocities superimposed on the elevation, for deforming volcanoes in which a larger view was not presented in the main manuscript. We can observe some correlations between the velocities and topography interpreted as atmospheric noise, but regions interpreted to be deforming display velocities of higher magnitudes than the noise and are uncorrelated to the topography (See Figures S11-S13).

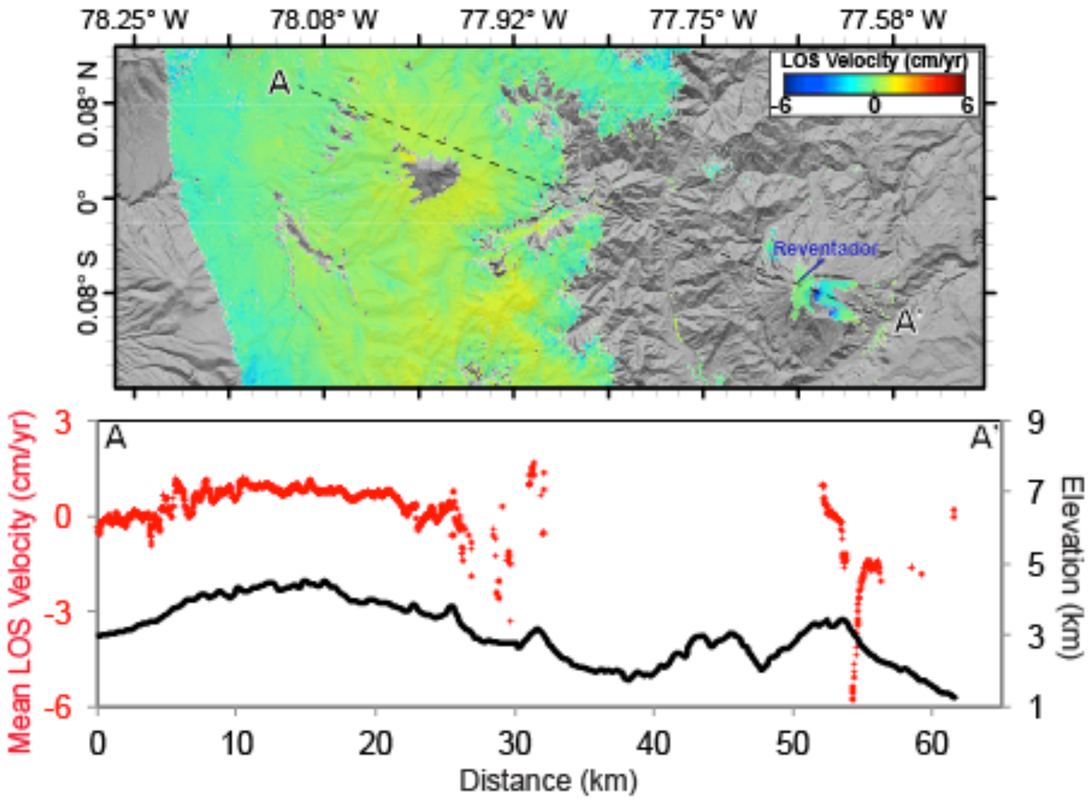

Figure S11. Mean 2007-2011 LOS velocity map over Reventador, with a profile through the region of subsidence and surroundings. The black dashed line indicates the location of the profile below that is superimposed on the topographic profile.

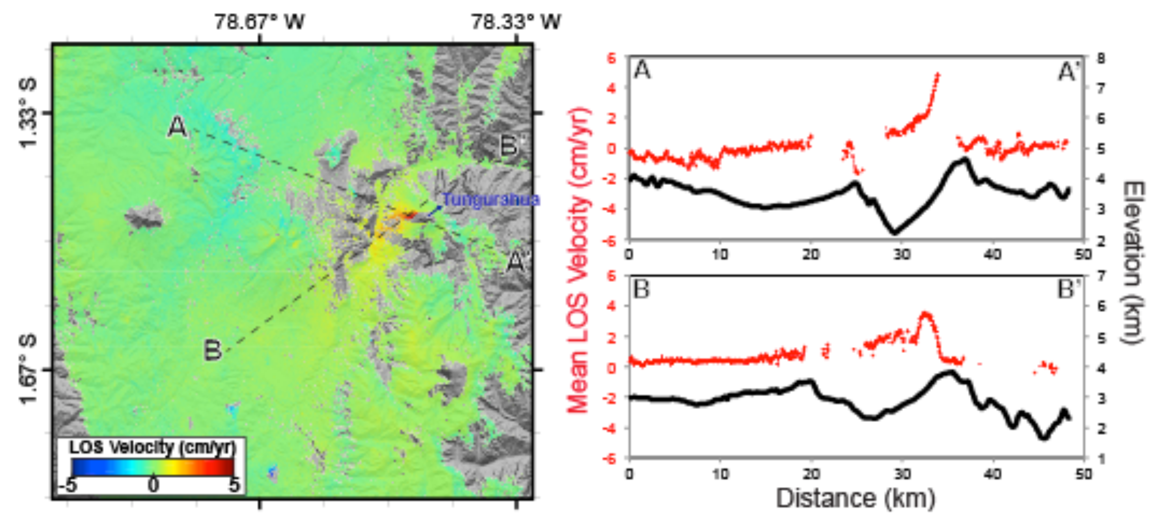

Figure S12. Same as Figure S11 but over Tungurahua, with profiles through the region of uplift and surroundings.

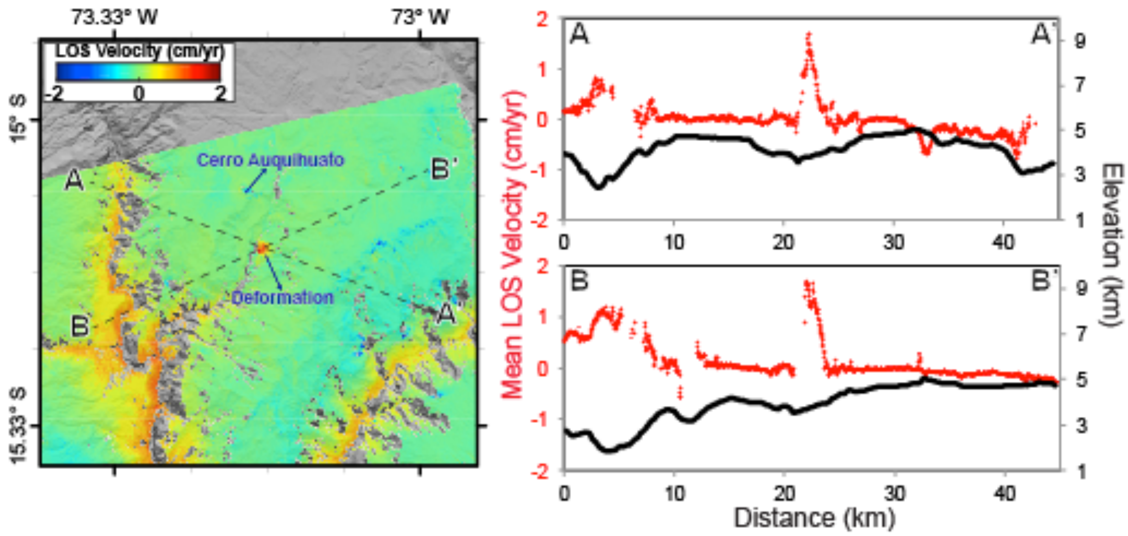

Figure S13. Same as Figure S11 but over Cerro Auquihuato region, with profiles through the region of uplift and surroundings.

Data Set S1. Satellite track, frame, and perpendicular baseline of interferograms used for this study.

References

Fattahi, H., and F. Amelung (2013), DEM Error Correction in InSAR Time Series, *Geoscience and Remote Sensing, IEEE Transactions on*, *51*(7), 4249-4259, doi:10.1109/TGRS.2012.2227761.

Siebert, L., and T. Simkin (2002-2015), Volcanoes of the world: an illustrated catalog of Holocene volcanoes and their eruptions, *Smithsonian Institution, Global Volcanism Program Digital Information Series*, *GVP-3*.